Acta Oceanol. Sin., 2017, Vol. 36, No. 9, P. 15–22
DOI: 10.1007/s13131-017-1106-z
http://www.hyxb.org.cn
E-mail: hyxbe@263.net

The analysis of gales over the "Maritime Silk Road" with remote sensing data

LIU Yuanxin[1], YIN Xiaobin[2]*, XU Youping[3]

[1] College of Computer, National University of Defense Technology, Changsha 410073, China

[2] Marine Department, Beijing Piesat Information Technology Co. Ltd, Beijing 100195, China

[3] The State Key Laboratory of Numerical Modeling for Atmospheric Sciences and Geophysical Fluid Dynamics (LASG), Institude of Atmospheric Physics (IAP), Chinese Academy of Sciences, Beijing 10029, China

Received 4 February 2017; accepted 23 March 2017

Abstract

The 21st century "Maritime Silk Road" strategy is a significant part of the belt and road initiatives of China. The cognition and investigation of ocean environment is essential and necessary in these regions which will provide scientific reference for many fields such as navigation, ocean engineering, and disaster prevent and reduction. A high-resolution cross-calibrated multi-platform wind product is used to analyze gales over the Maritime Silk Road. The yearly mean speed and space distribution of gale, and the frequencies and trends of gale and extreme wind speed are analyzed. The results show that relatively high pools of gale are mainly located in the waters of the Arabian Sea, the Somali Sea, Indo-China Peninsula sea area, and Bay of Bengal in the summer. The gale frequency of the Somali Sea is more than 90%. Overall, the gale days increase year by year in the majority of the South China Sea and the northern Indian Ocean, especially in the autumn and the winter.

Key words: Maritime Silk Road, gale, climate change, trend

Citation: Liu Yuanxin, Yin Xiaobin, Xu Youping. 2017. The analysis of gales over the "Maritime Silk Road" with remote sensing data. Acta Oceanologica Sinica, 36(9): 15–22, doi: 10.1007/s13131-017-1106-z

1 Introduction

The 21st century "Maritime Silk Road", as an important part of the belt and road initiatives, will establish a bridge for communication and cooperation between China and the Association of Southeast Asian Nations (ASEAN). Furthermore, it will profoundly influence the further integration of China and the ASEAN into the global economy. The "Maritime Silk Road" begins in Quanzhou (Fujian Province, China), and hit Guangzhou (Guangdong Province), Beihai (Zhuang Autonoraous Region of Guangxi Province, China), and Haikou (Hainan Province, China) before heading south to the Malacca Strait and other important harbors. The "Maritime Silk Road" is mainly located in the South China Sea and the northern Indian Ocean (Fig. 1). The South China Sea is a marginal sea that is the second most used sea lane in the world, and its importance results from one-third of the world's shipping transiting through its waters. The Indian Ocean provides major sea routes connecting the Middle East, Africa, and East Asia with Europe and the Americans, and it carries a particularly heavy traffic of petroleum and petroleum products from the oil fields of the Persian Gulf and Indonesia. So the study of the marine environment in these regions is necessary and it will contribute to the safety of the "Maritime Silk Road". An ocean surface wind is an important parameter of marine meteorology, and the systemic study of it can provide scientific advices and references for navigation, ocean engineering, harbor construction, and disaster prevent and reduction.

Based on the ship-borne data, Li et al. (2003) made some meteorological elements distribution charts such as average wind speed (WS), frog, and gale during the period of 1950 to 1995. Zheng et al. (2012) studied the ocean surface wind of the South China Sea and the Northern Indian Ocean using ERA-40 wind products from September 1957 to August 2002. They found that the wind was significantly affected by the monsoon and the sea surface WS has an obvious increasing tendency in the majority of the northern Indian Ocean. Based on the cross-calibrated multi-platform (CCMP) wind products, Zheng (2011) found that the sea surface WS in most areas of the South China Sea displayed obvious increasing tendency and extreme WS mainly lied in the north area of the South China Sea. Zheng (2013) also studied the seasonal characteristics of the gale frequency in the global ocean using 0.5°×0.5° OSCAT/NCEP blended ocean winds during a period from August 1999 to July 2009.

However, ship-borne data cannot provide enough temporal and spatial coverages and the WS from atmospheric models like ECMWF and NCEP is expected to be less accurate than those from remote sensing. Based on the high quality controlled CCMP wind products from short revisit and high temporal-spatial sampling remote sensing measurements with a long time series, the detailed analyses of the sea surface gale are performed for each month and season in this study in order to provide significant scientific references for the route-design of the "Maritime Silk Road". The time trend of gale and the characteristics of the extreme wind speed are studied in the Maritime Silk Road region for the first time ever. The study is organized as follows. In Section 2, the data and method are described. In Section 3, a detailed study is performed on the monthly distribution of the 24-

Foundation item: The National Natural Science Foundation of China under contract Nos 61501433 and Grant 412760.
*Corresponding author, E-mail: yinxiaobin@piesat.cn

Fig. 1. The "Maritime Silk Road" (http://www.conmatrix.com/ 2015/11/22/the-silk-road-economic-belt-and-the-21st-century-maritime-silk-road/).

year averaged sea surface winds and on the sea surface gale, including time and space the distribution of gale, the gale frequency and the time trend of gale and the distribution of the extreme WS. The results are summarized in Section 4.

2 Data and method

2.1 *CCMP wind product*

The CCMP ocean surface wind product is derived through the cross-calibration and assimilation of ocean surface wind data from SSM/I, TMI, AMSR-E, SeaWinds on QuikSCAT, and SeaWinds on ADEOS-II. These ocean surface wind data sets are created by combining the wind measurements obtained from multisatellite data. Recently, a consistent 24-year climate data record of a high resolution (0.25°×0.25°) sea surface wind vector can be achieved from the website (http://rda.ucar.edu/datasets/ds744.9/) for the period of July 1987 to December 2011. The period of the CCMP wind product is more than twice that of the OSCAT/NCEP blended product and the grid resolution of the CCMP wind product is four times better than that of the OSCAT/NCEP blended product. The detailed description document can be obtained from Atlas et al. (2011). All of the results in our study are based on the 6 h wind products (Level 3.0) from January 1988 to December 2011.

Compared with the *in situ* observations, the CCMP WS has an RMS speed difference ranging from 1.6 m/s versus ships to 0.6 m/s versus buoys (Atlas et al., 2011; Hoffman et al., 2013). The CCMP WS has an RMS difference of approximately 0.5 m/s over a period of 20 years, relative to a special sensor microwave imager (SSMI) data, and has an RMS difference of approximately 0.8 m/s relative to a quick scatterometer (QuikSCAT) data (Atlas et al., 2011; Hoffman et al., 2013).

2.2 *Method*

2.2.1 *Estimate of time trend*

To analyze a time series of data, a time trend coefficient can be obtained from

$$x_i = b + kt_i \quad (i = 1, \cdots, n), \tag{1}$$

where x_i is a series of measurements; t_i is a time series; n is the sample size; and k is the time trend coefficient which is calculated by a least square estimation.

2.2.2 *Gumbel distribution*

The Gumbel's (1954) statistical theory is always used to model the distribution of the maximum of a time series of measurements. The Gumbel distribution to represent the distribution of maxima relates to an extreme value theory, and it is useful in predicting the chance that flood, strong winds or other natural disaster will occur (Gumbel, 1941; Burke et al., 2010). When the samples and the frequency (P') are given, the extreme value can be calculated by

$$x_p = \left(\varphi \frac{S_X}{\bar{x}} + 1\right)\bar{x} = \left(\varphi \hat{C}_v + 1\right)\bar{x}, \tag{2}$$

where $\bar{x}$ is the mean value of samples, S_X is the sample variance; φ is the coefficient of deviation from mean, and it can be calculated by

$$\varphi = -\frac{\sqrt{6}}{\pi}\left\{0.577\ 22 + \ln\left[-\ln\left(1 - P'\right)\right]\right\}. \tag{3}$$

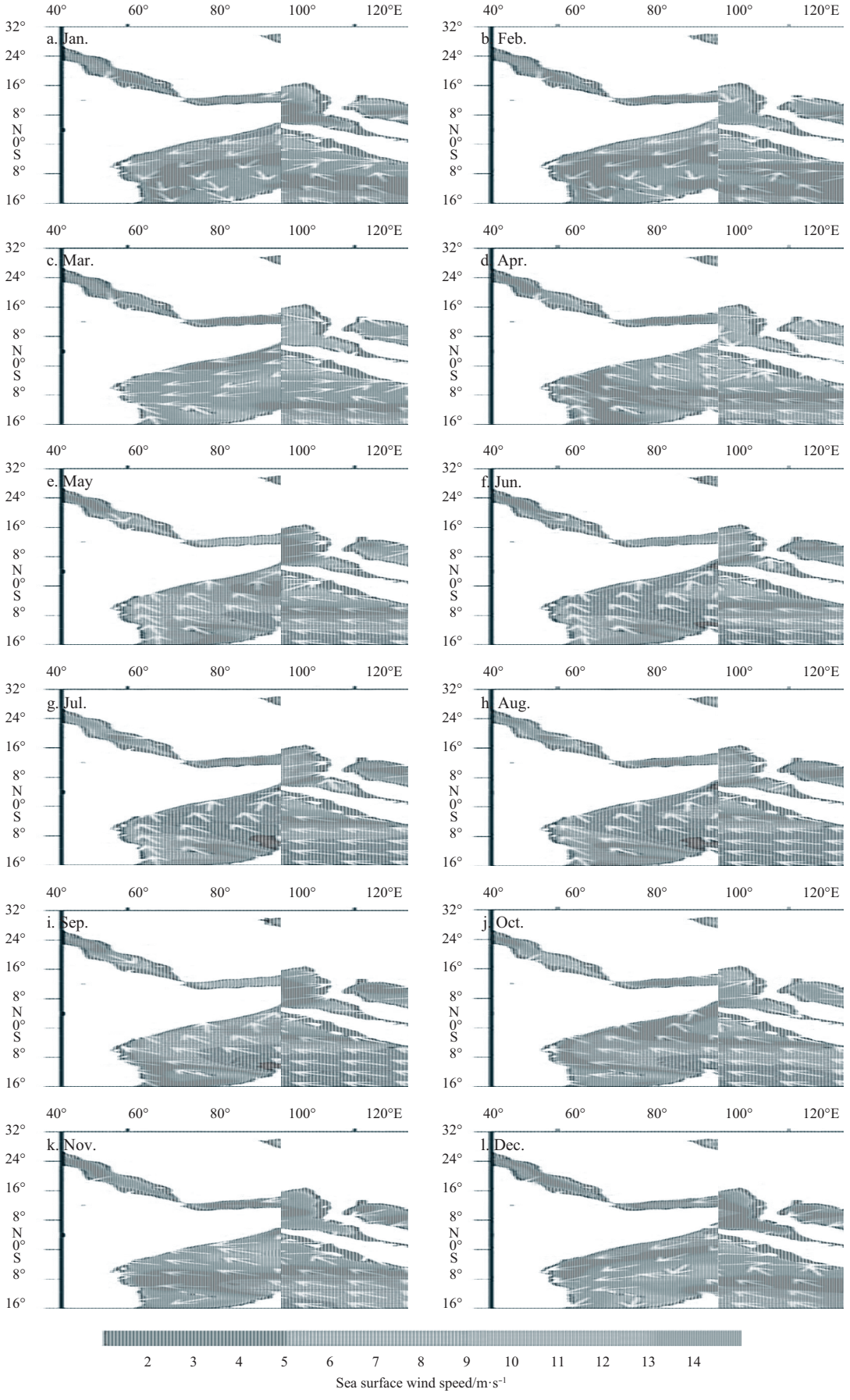

Fig. 2. The distribution of the 24-year averaged sea surface WS for each month from 1988 to 2011 over the Maritime Silk Road.

3 Results

3.1 *Monthly characteristics of wind*

The averaged wind vectors using the CCMP wind products from January 1988 to December 2011 for each month are shown in Fig. 2. Overall, the WS and the wind direction (WD) show obvious regional and monthly differences in the South China Sea and the northern Indian Ocean.

The characteristic of wind field during the MAM (March, April, and May in Fig. 2). In March, the average WS in the South China Sea is stronger than that of the northern Indian Ocean. There is a relatively high WS area near the Luzon Strait, and the predominant WD is from north and northeast. The WD shows a clockwise rotation in the Bay of Bengal. In April, the average WS tends to weaken gradually in the South China Sea and the northern Indian Ocean. The WD shows a clockwise rotation in the Arabian Sea and the Bay of Bengal again. In May, the southwest monsoon appears gradually in the most waters of the northern Indian Ocean and the southern part of the South China Sea. The two relatively high WS area are located in the Somali Sea and the Sri Lanka Sea, and the value is about 8.5 m/s.

The characteristics of the wind field during the JJA (June, July, and August) are described as follows. In June, the summer southwest monsoon is established in the Northern Indian Ocean and the South China Sea. The highest value (about 12.5 m/s) appears near the Somali Sea area. The Bay of Bengal has also a relatively high value area. In July, the summer southwest monsoon becomes stronger and the highest value (above) 13.5 m/s appears near the Somali Sea area and the southwest of the Arabian Sea. In August, the summer southwest monsoon continues to cover the northern Indian Ocean and the South China Sea. Overall, the average WS in the northern Indian Ocean is obviously stronger than that of the South China Sea in the summer.

The characteristics of the wind field during the SON (September, October, and November) are described as follows. In September, the southern part of the South China Sea and most of the northern Indian Ocean still show southwest wind, but the magnitude is lower than that in August. At this time, the two relatively high WS areas are located in the Somali Sea area and the Sri Lanka Sea area, and the values are about 10.5 and 9.5 m/s, respectively. In October, the magnitude of the WS in the northern Indian Ocean continues to weaken, but the South China Sea becomes strong gradually. In November, the most of South China Sea and the northern Indian Ocean show northeast wind, and the highest value of the WS is located near the Luzon Strait, above 10.5 m/s.

The characteristics of the wind field during the DJF (December, January, and February) are described as follows. In December, the east monsoon is prevailing, and the high value appears in the Luzon Strait and the Indo-China Peninsula sea area. The average WS in the South China Sea is stronger than that of the northern Indian Ocean. In January, the relatively high WS center appears in the Luzon Strait, the Taiwan Strait, and the Indo-China Peninsula sea area. In February, the magnitude of WS weakens to about 7 m/s in the South China Sea and weakens to about 5 m/s in the northern Indian Ocean.

3.2 *Analysis of sea surface gale*

3.2.1 *Frequency characteristics of ocean surface gale*

The 24-year averaged gale (more than 10.8 m/s: 6 grade, the same hereinafter) frequency analyzed using the CCMP wind products from January 1988 to December 2011 is shown in Fig. 3.

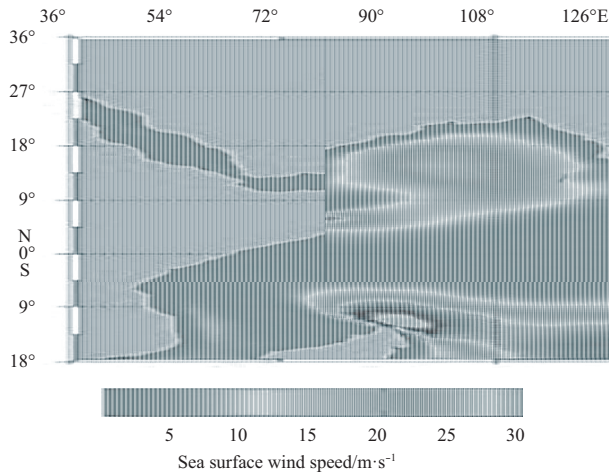

Fig. 3. The frequency distribution of the 24-year averaged ocean surface gale from 1988 to 2011 over the Maritime Silk Road.

Overall, the gale frequency shows obvious regional differences in the study area. The Somali Sea and the southwest of the Arabian Sea have an obvious relatively high frequency area with a value above 29%. The Luzon Strait and the Taiwan Strait have also an obvious relatively high frequency area with a value above 27%. In addition, the two relatively high value areas are located in the Indo-China Peninsula sea area and the Sri Lanka sea area. Overall, the average gale frequency in the South China Sea is stronger than that of the northern Indian Ocean.

3.2.2 *Seasonal characteristics of ocean surface gale*

The seasonal characteristics of the gale frequency are shown in Fig. 4, including the spring (MAM: March, April, and May), summer (JJA: June, July, and August), autumn (SON: September, October, and November), and winter (DJF: December, January, and February). In spring, the gale frequency is low in the majority of the South China Sea and the northern Indian Ocean. The relatively high regions of the gale frequency are found in the Taiwan Strait (above 9%) and the Luzon Strait (above 9%). In summer, the highest value (above 90%) appears near the Somali Sea area and southwest of the Arabian Sea, which may be due to the influence of summer southwest monsoon. In addition, three relatively high value regions are also found in the Bay of Bengal (above 20%), the Indo-China Peninsula sea area (above 15%), and the Sri Lanka sea area (above 15%). In autumn, the gale frequency of the Somali Sea area weakens to about 12%. On the contrary, the gale frequency of the South China Sea becomes strong gradually, and the highest value center is more than 32%. In winter, the gale frequency of the South China Sea becomes stronger that may be due to the activity of cold air during DJF, and the highest value center is more than 45% in the Luzon Strait. At this time, the gale frequency of the northern Indian Ocean is less than 5%.

3.2.3 *Monthly characteristics of ocean surface gale*

The monthly characteristics of the gale frequency are shown in Fig. 5. The characteristics of the ocean surface gale during the MAM (March, April, and May) are described as follows. In March, the gale frequency of the northern Indian Ocean is less than 4%. The relatively high value regions appear in the Luzon Strait (above 20%) and the Taiwan Strait (above 16%). In April, the gale frequency gradually decreases in the South China Sea,

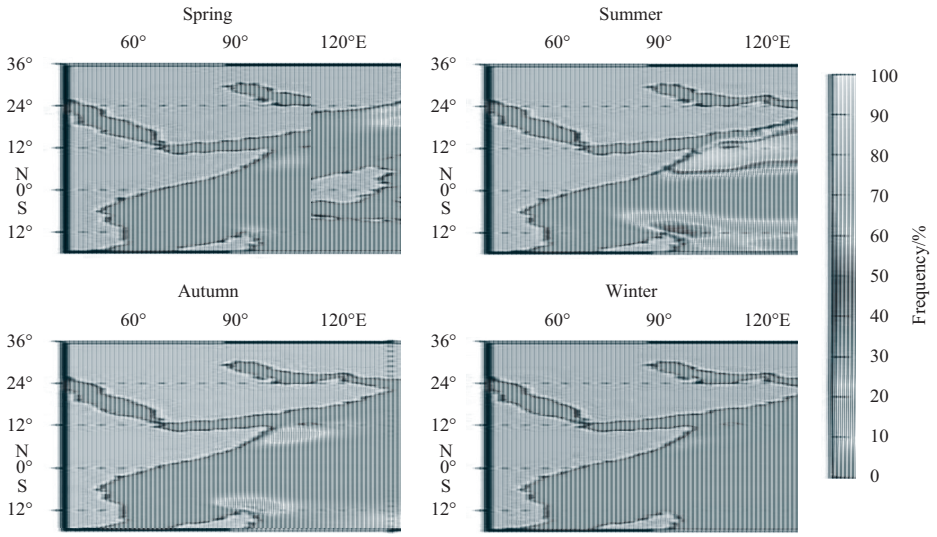

Fig. 4. The frequency distribution of the 24-year averaged ocean surface gale for each season from 1988 to 2011 over the Maritime Silk Road.

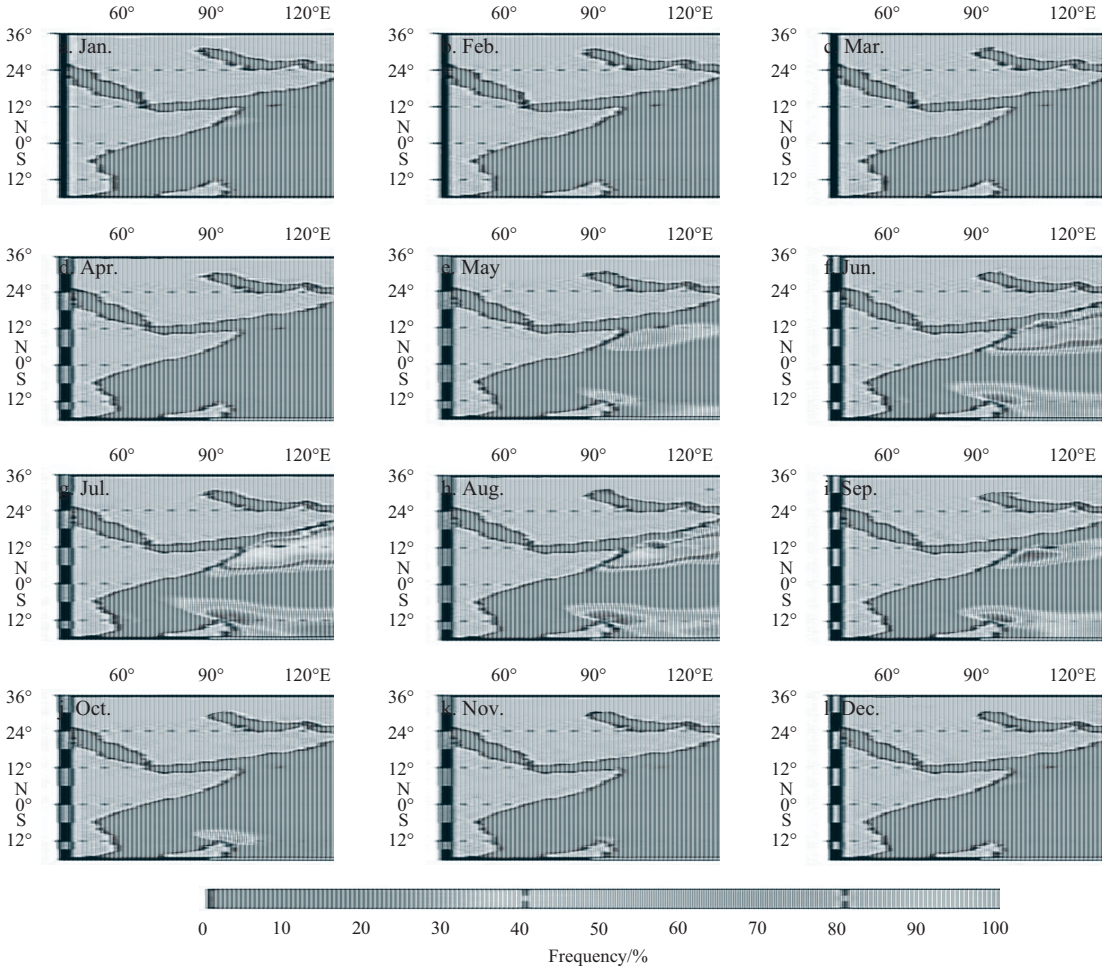

Fig. 5. The frequency distribution of the 24-year averaged ocean surface gale for each month from 1988 to 2011 over the Maritime Silk Road.

and that of the northern Indian Ocean is below 3%. In May, the two relatively high value regions are found in the Somali Sea area (above 20%) and the Sri Lanka Sea area (above 15%). At this time, the gale frequency of the South China Sea is less than 4%.

The characteristics of the ocean surface gale during the JJA (June, July, and August) are described as follows. In June, the

highest gale frequency center appears near the Somali Sea area and the southwest of the Arabian Sea, and the frequency is above 80%. The Bay of Bengal has also a relatively high value (above 20%) area. In July, the summer southwest monsoon becomes strong gradually and the highest gale frequency is more than 90% near the Somali Sea area and the southwest of the Arabian Sea, which is similar to the analysis of Zheng (2013). The gale frequency increases gradually near the Indo-China Peninsula sea area. In August, the gale continues to cover the most of the northern Indian Ocean and the Indo-China-Peninsula sea area.

The characteristics of ocean surface gale during the SON (September, October, and November) are described as follows. In September, the magnitude of gale becomes weak in the South China Sea and the northern Indian Ocean. In October, the gale frequency of the northern Indian Ocean is less than 3%. At this time, the gale frequency becomes strong gradually in the northern part of the South China Sea. In November, the gale frequency continues to strengthen in the northern part of the South China Sea and the frequency is above 42%.

The characteristics of ocean surface gale during the DJF (December, January, and February) are described as follows. In December, the gale frequency of the South China Sea is found above 40% and in the highest value center there is above 60%. The gale frequency is low in the northern Indian Ocean. In January, the gale frequency weakens gradually in the South China Sea. The relatively high value regions are located in the Taiwan Strait, the Indo-China Peninsula sea area, and the Luzon Strait. In February, the gale frequency continues to weaken in the South China Sea.

3.2.4 *Time trend of gale days*

In order to analyze the long-term variation of the ocean gale, the gale days of each grid has been calculated for each year. The trend is quantified as a linear function over the duration of the time series (Eq. (1)), and the time trend coefficient is calculated by the least square estimation. It should be noted that the shaded areas passed 95% confidence level test. As shown in Fig. 6, the gale days are increasing in the most regions of the South China Sea and the northern Indian Ocean during the last 24 years. The regional difference is obvious. Waters with obvious linear increasing trend (about 2.0–4.5 d/a) mainly are located in the majority of the South China Sea such as the Taiwan Strait, the Luzon Strait, and the Indo-China Peninsula sea area. In addition, the Sri Lanka Sea area and the Somali Sea area have also an obvious increasing trend (about 1.5–2.5 d/a). The increasing trend is also found in the waters of the Bay of Bengal and the northern part of the Arabian Sea (about 0.5–1 d/a).

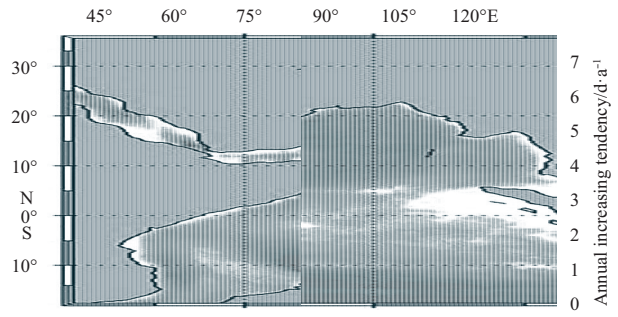

Fig. 6. The annual increasing tendency of gale days from 1988 to 2011 over the Maritime Silk Road. The shaded areas passed 95% confidence level test.

As shown in Fig. 7, the calculated trend of gale days is depicted in different months. The regional and monthly differences are obvious. It should be noted that the shaded areas passed 95% confidence level test. It can be seen from Fig. 6, the obvious linear increasing trend is found in the majority of the South China Sea (January, March, and December), and the most notable waters are located in the Taiwan Strait. The relatively obvious linear increasing trend is also found in the majority of the Bay of Bengal in May, June, July, August and September. The two obvious linear increasing trends are found in the northern part of the Arabian Sea in June and August. Waters with relatively obvious linear increasing trend are also located in the Somali Sea area in May, June, August, September, and December.

3.3 *Characteristics of extreme wind speed*

The strong winds in the sea usually bring heavy death and economic loss. So the study of the extreme WS is necessary. As shown in Fig. 8, the distribution of the 24-year averaged extreme WS is performed using the CCMP wind products during the period from 1988 to 2011. The relatively high value (above 18 m/s) waters are located in the majority of the South China Sea, the Somali Sea area (above 18 m/s) and the southwest of the Arabian Sea (above 18 m/s), and the northern part of the Bay of Bengal (above 16 m/s). The magnitude of the extreme WS is more than 21 m/s near the Taiwan Strait and the Luzon Strait. Overall, the extreme WS in the South China Sea is stronger than that of the northern Indian Ocean. The extreme WS is relatively low near the equator.

4 Summary

In this paper, we performed a detailed and systematic analysis of the ocean surface gale, including the yearly, seasonal and monthly mean winds distributions, time and space distributions of gale, the gale frequency, the time trend of gale and the extreme WS in the 21st "Maritime Silk Road" region. Thanks to the 24-year long time series and the 0.25°×0.25° high grid resolution of the CCMP wind product, more regional characteristics of gales are noticed than the previous studies. The main conclusions are as follows:

The 24-year averaged WS and WD show some obvious regional and monthly characteristics in the South China Sea and the northern Indian Ocean. During the MAM, the magnitude of WS is relatively weak in the majority of the South China Sea and the northern Indian Ocean. During the JJA, the highest WS center is located in the Somali Sea area. At this time, the summer southwest monsoon covers these regions. During the SON, the WS becomes weak in the majority of the northern Indian Ocean, but that becomes strong in the most regions of the South China Sea. During the DJF, the highest WS center is located in the northern part of the South China Sea.

Overall, the gale frequency shows obvious regional differences in the studied area. The obvious high value areas are located in the Somali Sea area and the southwest of the Arabian Sea, the Luzon Strait, the Taiwan Strait, and the Indo-China Peninsula sea area. In addition, the seasonal and monthly differences are also noticeable. For example, in spring, the gale frequency is low in the majority of the South China Sea and the northern Indian Ocean. In summer, the highest value (above 90%) appears near the Somali Sea area and southwest of the Arabian Sea, but it is relatively weak in winter. In winter, in the highest value center there is more than 45% in the Luzon Strait, however, it is relatively weak in the summer.

The gale days are increasing in the most regions of the South

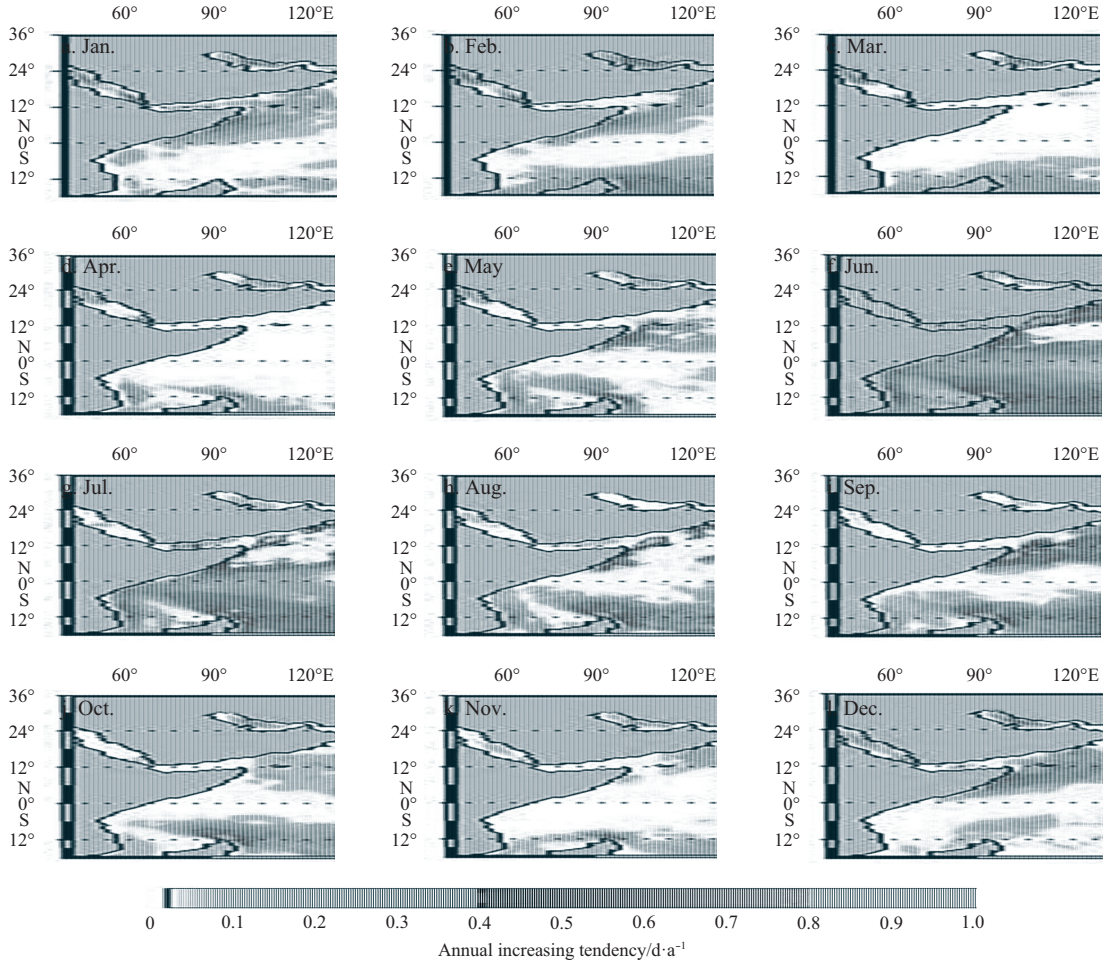

Fig. 7. The annual increasing tend of gale days for each month from 1988 to 2011 over the Maritime Silk Road. The shaded areas passed 95% confidence level test.

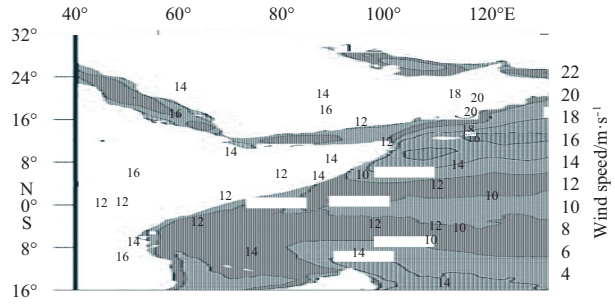

Fig. 8. The distribution of the 24-year averaged extreme sea surface WS from 1988 to 2011 over the Maritime Silk Road.

China Sea and the northern Indian Ocean during the last 24 years, and the regional difference is obvious. Waters with an obvious linear increasing trend mainly are located in the majority of the South China Sea such as the Taiwan Strait, Luzon Strait, and the Indo-China Peninsula sea area. The increasing trend is also found in the waters of the Bay of Bengal and the northern part of the Arabian Sea. In addition, the monthly difference is also obvious. The increasing trend of gales in the "Maritime Silk Road" is likely related to the global climate change and needs more analysis in the future. Overall, the extreme WS in the South China Sea is stronger than that of the Northern Indian Ocean. The extreme WS is relatively low near the equator.

Acknowledgements

The authors thank the Research Data Archive at the National Center for Atmospheric Research, Computational and Information Systems Laboratory for providing Cross-Calibrated multiplatform ocean surface wind velocity (http://rda.ucar.edu/datasets/ds744.9/).

References

Atlas R, Hoffman R N, Ardizzone J, et al. 2011. A cross-calibrated, multiplatform ocean surface wind velocity product for meteorological and oceanographic applications. Bulletin of the American Meteorological Society, 92(2): 157–174

Burke E J, Perry R H J, Brown S J. 2010. An extreme value analysis of UK drought and projections of change in the future. Journal of Hydrology, 388(1–2): 131–143

Gumbel E J. 1941. The return period of flood flows. The Annals of Mathematical Statistics, 12(2): 163–190

Gumbel E J. 1954. Statistical Theory of Extreme Values and Some Practical Applications: Applied Mathematics Series 33. Washington, DC: U S Govt Print Office

Hoffman R N, Ardizzone J V, Leidner S M, et al. 2013. Error estimates for ocean surface winds: applying desroziers diagnostics to the cross-calibrated, multiplatform analysis of wind speed. Journal of Atmospheric and Oceanic Technology, 30(11): 2596–2603

Li Pei, Zhang Xian, Yu Mugeng. 2003. Climate characteristic analyze

of in North Indian Ocean. Marine Forecasts (in Chinese), 20(3): 25–30

Zheng Chongwei. 2011. Sea surface wind field analysis in the China sea during the last 22 years with CCMP wind field. Meteorology and Disaster Reduction Research (in Chinese), 34(3): 41–46

Zheng Chongwei. 2013. Statistics of gale frequency in global oceans. Journal of Guangdong Ocean University (in Chinese), 33(6): 77–81

Zheng Chongwei, Li Xunqiang, Pan Jing. 2012. Wave climate analysis of the South China Sea and North Indian Ocean form 1957 to 2002. Journal of Oceanography in Taiwan Strait (in Chinese), 31(3): 317–323